ACS Sustainable Chemistry & Engineering

Research Article

pubs.acs.org/journal/ascecg

# Low Temperature $CO_2$ Methanation: ZIF-67-Derived Co-Based Porous Carbon Catalysts with Controlled Crystal Morphology and Size

Wenhui Li,[†] Anfeng Zhang,[†] Xiao Jiang,[‡] Chen Chen,[†] Zhongmin Liu,[§] Chunshan Song,*[,†,‡] and Xinwen Guo*[,†]

[†]State Key Laboratory of Fine Chemical, PSU-DUT Joint Center for Energy Research, Faculty of Chemistry, Dalian University of Technology, Dalian 116024, P. R. China

[‡]Clean Fuels & Catalysis Program, PSU-DUT Joint Centre for Energy Research, EMS Energy Institute, Pennsylvania State University, University Park, Pennsylvania 16802, United States

[§]National Engineering Laboratory for Methanol to Olefins, Dalian National Laboratory for Clean Energy, Dalian Institute of Chemical Physics, Chinese Academy of Sciences, Dalian 116023, P. R. China

Supporting Information

**ABSTRACT:** A Co-based zeolitic imidazolate framework, ZIF-67, has been utilized as a precursor to obtain Co-based porous carbon catalysts. The obtained catalysts display an outstanding catalytic performance toward the $CO_2$ methanation at low temperature. The ZIF-67 crystal morphology can be controlled from cubic to rhombic dodecahedron, and the original particle sizes can be regulated from 150 nm to 1 $\mu$m in aqueous solution by cetyltrimethylammonium bromide (CTAB) surfactants. After carbonation in $N_2$ flow, Co-based porous carbon catalysts kept the original ZIF-67 crystal morphology and particle size but differed in the micropore property; the 0.01 wt % CTAB content led to the maximum micropore volume 0.125 $cm^3/g$. The Co nanoparticles inside the carbon matrix range between 7 and 20 nm, and they are separated by the graphite-like carbon avoiding the metal sintering effectively. Furthermore, the catalysts with 0.01% CTAB addition exhibited the highest $CO_2$ conversion (52.5%) and $CH_4$ selectivity (99.2%) under the 72000 mL $g^{-1}$ $h^{-1}$ GHSV (gas hourly space velocity) at 270 °C. Noticeably, the Co/PC catalysts performed higher activity and stability than the supported catalysts 20Co/AC. The versatile way offers good prospects for low temperature $CO_2$ methanation and prevents metal sintering effectively.

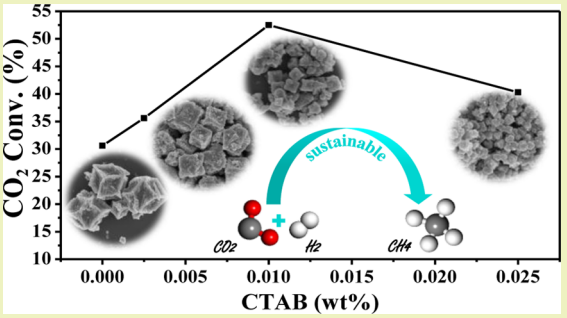


**KEYWORDS:** *$CO_2$ methanation, Low-temperature, ZIF-67, CTAB, Cobalt*

## INTRODUCTION

Due to the pernicious effects of the greenhouse gases on global warming, $CO_2$ utilization has received considerable attention,[1] in which hydrogenation of $CO_2$ is an efficient approach to reduce $CO_2$ emission.[2−10] $CH_4$, a product of $CO_2$ hydrogenation, is the main component of liquefied natural gas (LNG), which has been widely used in the present combustion systems. In the ammonia synthesis and fuel cell industries, $CO_2$ methanation can prevent catalyst poisoning through the elimination of CO from $H_2$-rich gas flow.[11] In addition, the Sabatier reaction is also regarded as a method in oxygen regeneration within life support systems.[12,13] $CO_2$ methanation is an exothermic reaction with high effectivity on account of the high equilibrium $CO_2$ conversions at 25 to 400 °C. $CO_2$ methanation over inexpensive and stable catalysts is a promising new way to store the renewable energy such as wind and solar power, to transform biogas effectively to biomethane, and to convert $CO_2$ to chemical feedstock and fuel. To date, most research has focused on the $CO_2$ methanation over traditional metal-supported catalysts, e.g., Co,[14] Ni,[15] Ru,[16] Rh,[17] and Pd[18] catalysts. Nonetheless, the noble metals still face difficulty in their large-scale application in industry for their high cost, despite the excellent hydrogenation performance; on the other hand, at a high reaction temperature (ca. 400 °C), the inexpensive Ni-based catalysts exhibit high $CO_2$ conversion and $CH_4$ selectivity, but rapid deactivation appears due to the metal particles sintering under high temperature and carbon deposition.[19] Hence, highly efficient catalysts at low reaction temperature are urgently needed.[20] Zhou et al.[21] prepared ordered mesoporous Co/KIT-6 for $CO_2$ methanation with the $CO_2$ conversion change from 15.5% to 48.9% when the reaction temperatures were in the range of 200 to 280 °C. Zhou et al.[22] also synthesized Ni/$CeO_2$ catalyst for $CO_2$ methanation with 44% $CO_2$ conversion at 260 °C at 22000 mL/($g_{cat}$·h). Wierzbicki et al.[23] tested Ni−La-hydrotalcite catalysts at temperatures from 250 to 300 °C for $CO_2$

Received: April 26, 2017
Revised: July 27, 2017
Published: August 1, 2017






DOI: 10.1021/acssuschemeng.7b01306
ACS Sustainable Chem. Eng. 2017, 5, 7824−7831

methanation, and $CO_2$ conversion varied from 46.5% to 75% at 12000 mL/($g_{cat}$·h). The supported catalysts are superior in numerous aspects, like mechanical stability, but limited by the dispersion and sintering of active metal so that high surface area and antisintering materials are imperative.

MOFs have been widely applied in catalysis, gas adsorption and storage, and chemical sensors, etc.[24−26] In addition, MOFs with high surface area are also applied as the catalysts supports.[27,28] Zhen et al.[29] used MOF-5 as the catalyst support to increase the Ni dispersion for $CO_2$ methanation with 47.2% $CO_2$ conversion at 280 °C. In our previous work,[30] ZIF-8 and MIL-53(Al) had been used as supports for $CO_2$ hydrogenation and showed an outstanding performance in comparison with $\gamma$-$Al_2O_3$. However, MOFs are unfavorable for the high-temperature reaction for their instability under the hydrothermal reaction condition. It should also be mentioned that thermal decomposition is an alternative strategy and research direction to get the stable carbon porous materials using MOFs as hard templates.[31−33] Composites obtained by thermal decomposition of MOFs possess the synergistic interaction between highly dispersed metal nanoparticles and the nanoporous carbon matrix.[34] In the solid−solid transformation process, the porosity and morphology can be partially preserved.[32] Zhou et al.[33] have carbonized ZIF-67 to afford Co NPs for the oxidation of alcohols, which exhibits an outstanding performance; the active Co NPs were formed directly during the thermal decomposition obtained by the $H_2$ hydrogenation on the supported catalysts.[33]Shen et al.[31] have developed Co@Pd core−shell NPs for nitrobenzene hydrogenation, which was more active than the Pd NPs supported on ZIF-67 and MIL-101. Futhermore, the metal nanoparticles derived from the carbonization of MOFs are wrapped by the graphitized carbon, which can effectively prevent the metal sintering.[35]

The adjustable morphologies and particle sizes can further facilitate the potential applications,[36,37] e.g., the crystal size decrease will give the enhancive surface area and reduced diffusion resistance.[38] The surfactants are usually used to tune the size and shape of MOFs crystals. Do et al. changed the size and shape of Fe-MIL-88B-$NH_2$ crystals by using surfactant nonionic triblock copolymer F127,[39] while Lai et al. used cetyltrimethylammonium bromide (CTAB) to control the ZIF-8 crystal size and morphology.[36] Pang et al. reported a synthesis method to obtain the shape-controlled Fe-MIL-88B particles by using a surfactant (polyvinylpyrrolidone, PVP).[40]

This work investigates MOF-derived catalysts with different morphologies and particle sizes for $CO_2$ methanation. In the present work, cetyltrimethylammonium bromide (CTAB) surfactants are added to the original solution to regulate the morphologies and particle sizes which is able to alter the $CO_2$ adsorption ability. Also, the ZIF-67-templated porous carbon and Co NPs exhibit excellent catalytic activity and selectivity toward $CO_2$ methanation at low reaction temperatures.

## EXPERIMENTAL SECTION

**ZIF-67 Preparation.** ZIF-67 nanoparticles were prepared as reported in the literature.[36] The chemicals were provided by Sigma-Aldrich. Typically, 0.29 g of cobalt nitrate hexahydrate was paired with a 10 mL aqueous solution, followed by 4.54 g of 2-methylimidazole and 0.0025, 0.01, and 0.025 wt % CTAB dissolved in 70 mL of deionized (DI) water. Subsequently, the cobalt nitrate and 2-methylimidazole solutions were mixed together at room temperature, and the synthesized solution was heated up to 120 °C for 6 h in Teflon-lined autoclaves. After synthesis, the ZIF-67 particles were separated from the solution by centrifuging and washed with methanol 3 times, followed by drying in the vacuum oven (−0.8 MPa) at 60 °C overnight.

**Preparation of Porous Carbon Catalysts Incorporating Co NPs.** Before the catalyst preparation, the thermal stability of ZIF-67 was investigated by thermogravimetric analysis (TGA) (see Figure S1). The weight began to reduce at 370 °C in air and 570 °C in nitrogen. In order to acquire the porous carbon materials, the temperature should be higher than 570 °C if nitrogen is selected as the carrier gas. Hence, the thermal decomposition temperature program is determined as follows. Before starting the temperature program, $N_2$ (ca. 60 mL/min) was introduced to discharge the air in the chamber for 120 min. Then, the chamber was heated up to 600 °C (700 °C, 800 °C) with a stepwise rate of 5 °C/min and kept for 120 min, followed by cooling down to room temperature. The catalysts that appeared in this work are denoted as Co/($x$)PC-$y$, where $x$ represents the mass fraction of the CTAB in the synthesis of ZIF-67, $y$ represents the carbonization temperature (°C), and PC stands for the porous carbon. The Co content in the Co-based porous carbon catalysts is listed in Table 1 and determined using TG analysis.

**Table 1. Co Content in the Co-Based Porous Carbon Catalysts**

| catalyst | Co (wt %)[a] |
|---|---|
| Co/(no)PC-600 | 33.5 |
| Co/(0.0025)PC-600 | 32.9 |
| Co/(0.01)PC-600 | 32.5 |
| Co/(0.025)PC-600 | 31.6 |
| Co/(0.01)PC-700 | 48.1 |
| Co/(0.01)PC-800 | 50.5 |

[a]The Co content in Table 1 was calculated through TG analysis. The TGA data were collected from 30 to 850 °C in an air flow.

**Preparation of Supported Catalyst Co/AC.** Commercially available activated carbon (bought from the Shenyang Xinxing Reagent Factory, China) was used as the support material. Co/AC catalyst was prepared by the impregnation method with an aqueous solution of $Co(NO_3)_2·6H_2O$ (>99%, Aladdin Chemicals) with Co loadings of 20 wt %. The obtained samples were dried at 120 °C for 12 h and calcined in $N_2$ flow (60 mL/min) at 600 °C for 4 h with a stepwise rate of 2 °C/min.

**Catalytic Test.** The $CO_2$ methanation was carried out in a fixed-bed flow reactor with 0.05 g of catalyst (10−20 mesh) for each test. Before the reaction, the catalyst was prereduced with $H_2$ at 400 °C and 3 MPa for 8 h. Then, the feed gas was switched to the mixture of $CO_2$ and $H_2$ with the $H_2/CO_2$ molar ratio of 4 under pressure of 3 MPa at 400 °C; the gas hourly space velocity was 72000 mL $g^{-1}$ $h^{-1}$.

The online gas chromatograph (FULI GC 97) was used to analyze the products. $CO_2$, CO, and $CH_4$ were analyzed with a thermal conductivity detector (TCD). The conversions of $CO_2$ and $CH_4$ selectivity were calculated as eqs 1 and 2

$$CO_2\ \text{conversion}\ (\%) = \frac{n_{CO_2,in} - n_{CO_2,out}}{n_{CO_2,in}} \times 100\% \quad (1)$$

$$CH_4\ \text{selectivity}\ (\%) = \frac{n_{CH_4,out}}{n_{CO_2,in} - n_{CO_2,out}} \times 100\% \quad (2)$$

where $n_{CO_2,in}$ and $n_{CO_2,out}$ represent the molar concentration of $CO_2$ in the feed and effluent, respectively; $n_{CH_4,out}$ represents the molar concentration of $CH_4$ in the effluent.

**Characterization of Catalysts.** XRD patterns were obtained by a RigakuSmartLab (9) diffractometer with Cu K$\alpha$ radiation ($\lambda$ = 1.5406 Å) from 5° to 80°.

The textural and sorption properties of the catalysts were received by $N_2$ adsorption on a Quantachrome AUTO-SORB-1-MP sorption analyzer at 77 K. Before the measurements, the samples were degassed at 300 °C for 2 h. The pore volume was estimated by the adsorbed



DOI: 10.1021/acssuschemeng.7b01306
ACS Sustainable Chem. Eng. 2017, 5, 7824−7831

volume at $P/P_0 = 0.95$. The micropore volume was calculated by the t-plot method. The $CO_2$ sorption properties of the samples were obtained by $CO_2$ adsorption on the same instrument at 298 K.

Scanning electron microscopy (SEM) images and energy dispersive spectrometer (EDS) maps were obtained with field emission scanning electron microscopy (NOVA NanoSEM 450). The samples were also studied with high resolution transmission electron microscopy (TEM) and scanning transmission electron microscopy/energy-dispersive X-ray spectroscopy (STEM/EDS) using a JEM-2100F instrument (JEOL Company).

Thermogravimetric analysis (TGA) was conducted on a TGA/SDTA851e thermobalance (Mettler Toledo). The TGA data were received between 30 and 850 °C in $N_2$ or air flow. The heating rate was 10 °C $min^{-1}$ at a flow rate of 25 mL/min. The weight change of spent catalysts was obtained by TG analysis.

Raman patterns were recorded on a DRX Raman Microscope ($\lambda$ = 532 nm).

The reducibility of the catalysts was analyzed by $H_2$-temperature-programmed reduction (TPR) with ChemBETPulsar TPR/TPD equipment (Quantachrome, USA). Prior to reduction, an ~0.10 g sample was charged into the quartz tube and flushed with high purity Ar at 300 °C for 1 h. The TPR program was then initiated by switching to 5 vol % $H_2$/Ar with a total flow rate of 30 mL $min^{-1}$ and heating up to 850 °C at 10 °C $min^{-1}$.

## RESULTS AND DISCUSSION

**Synthesis and Carbonization of ZIF-67 with Different Crystal Morphologies and Sizes.** ZIF-67 crystals morphologies and sizes were regulated with 0, 0.0025, 0.01, and 0.025 wt % CTAB addition. The XRD patterns (Figure 1) of the samples show the typical ZIF-67 crystals compared with previous reports.[41,42]

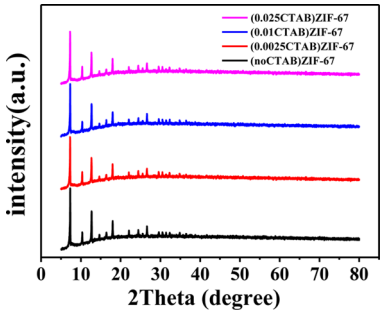


**Figure 1.** XRD patterns of ZIF-67 with different amounts of CTAB.

Figure 2a(1−4) show the SEM and TEM images of morphology-controlled ZIF-67 crystals obtained by different amounts of CTAB addition. Rhombic dodecahedron (RD) ZIF-67 was synthesized without CTAB, and the particle size is about 1 $\mu$m (Figure 2(a-1)). When the CTAB addition was increased to 0.0025 wt %, the morphology turns to truncated rhombic dodecahedron (TRD), and the average particle size decreases slightly (Figure 2(a-2)). With a further increase of CTAB to 0.01 wt %, the morphology changes to truncated cubes (TC), and the mean particle size decreases to ca. 250 nm (Figure 2(a-3)). The truncated cubic morphology is still maintained in the case of 0.025 wt % CTAB addition, while the particles become smaller (Figure 2(a-4)). Furthermore, the statistical graphs of the particle size distribution are shown in the insets in Figure 2a. In contrast to the broadened distribution, when the CTAB addition is up to 0.01 wt %, the particles size is concentrated in a narrow range. Seen from the crystal size distributions floated on the SEM images (Figures 2a and 2b), as the amount of CTAB is greater than 0.01 wt %, the uniformity is much better than the ZIF-67 particles free of CTAB addition.

The $N_2$ adsorption results of samples give BET surface area and microporous volume as tabulated in Table S1, and the pore size distribution is shown in Figure S2. The crystal size monotonically decreases with the increase of the CTAB addition, while the surface area reaches the maximum 1420 $m^2/g$ when the amount of CTAB is 0.01 wt %, as well as the microporous volume 0.519 $cm^3/g$. Consequently, the crystal morphology is dependent upon the concentration of CTAB and adjusted from rhombic dodecahedron to truncated cube, and the crystal size decreases from micrometer to nanometers.[36]

The prepared ZIF-67 were carbonized under $N_2$ flow and then characterized by SEM and TEM. Even after carbonization, the obtained catalysts inherit the original morphologies of ZIF-67 crystals with the distorting particle surface (Figure 2 b-c). Figure 2c shows that each Co/PC particle exhibits a highly porous structure. As seen in Figure 2d, the nanoparticles disperse well without obvious serious aggregation; the existence of crystallized Co nanoparticles is further confirmed by the high-resolution TEM image (Figure 3). The Co particle size decreases simultaneously with the decrease of the original ZIF-67 particle size; when the amount of CTAB is 0.01 wt %, the Co nanoparticle inside the carbon matrix is around 7 nm. From Figure 3, the graphene-like structure is observed. To study the correlation of the crystallization degree of graphitic carbon with the carbonization temperature, the Co/PC samples, carbonized at different temperatures, were analyzed by Raman spectroscopy (Figure 4). The disorder-induced D band (1350 $cm^{-1}$) and the C−C stretching G band (1580 $cm^{-1}$) are observed for all samples. The relative ratio of these two bands ($I_G/I_D$) could give information about the crystallization degree of graphitic carbon.[34] As shown in Figure 4, the relative ratio of G bands to D bands ($I_G/I_D$) on Co/(0.01)PC-600 particles is 0.61 and increases to 0.83 for Co/(0.01)PC-800 particles, indicating that graphitic structures are well developed. As the carbonization temperature increases, the crystallization degree of graphitic carbon increases.

The broadened and less-resolved peaks are observed on the Co/PC samples (Figure 5), which are in contrast to the sharp peaks of the original ZIF-67 crystals. As seen in Figure 5, the main diffractions are assignable to Co *fcc* and *hcp* crystals,[43] and with the gradual increase of carbonization temperature to 800 °C, diffraction peaks become more intense, indicating the larger Co crystal size. Though XRD patterns show no characteristic peaks of CoO, the oxygen element was observed on the EDS maps (see Figure S3), which indicates the existence of CoO. $H_2$-TPR profiles (Figure S4) give the reducibility of the cobalt oxides on the samples.

The specific surface areas and micropore volumes of carbonized Co/PC particles were determined by $N_2$ adsorption at 77 K and summarized in Table 2. The Co/(0.01)PC-600 has the maximum BET surface area 346 $m^2/g$ and the micropore volume 0.125 $cm^3/g$. The micropore volume decreases sharply to 0.083 $cm^3/g$ with the increase of carbonization temperature from 600 to 800 °C. The pore size distribution of Co/PC (see Figure S5) shows that the Co/(0.01)PC-600 possesses the smallest micropore (e.g., < 1 nm). More interestingly, compared to the original ZIF-67 crystals, the pores around 4 nm disappear.

The $CO_2$ adsorption capacity of the carbonized samples was also tested at 25 °C, and corresponding isotherms are depicted


DOI: 10.1021/acssuschemeng.7b01306
ACS Sustainable Chem. Eng. 2017, 5, 7824−7831

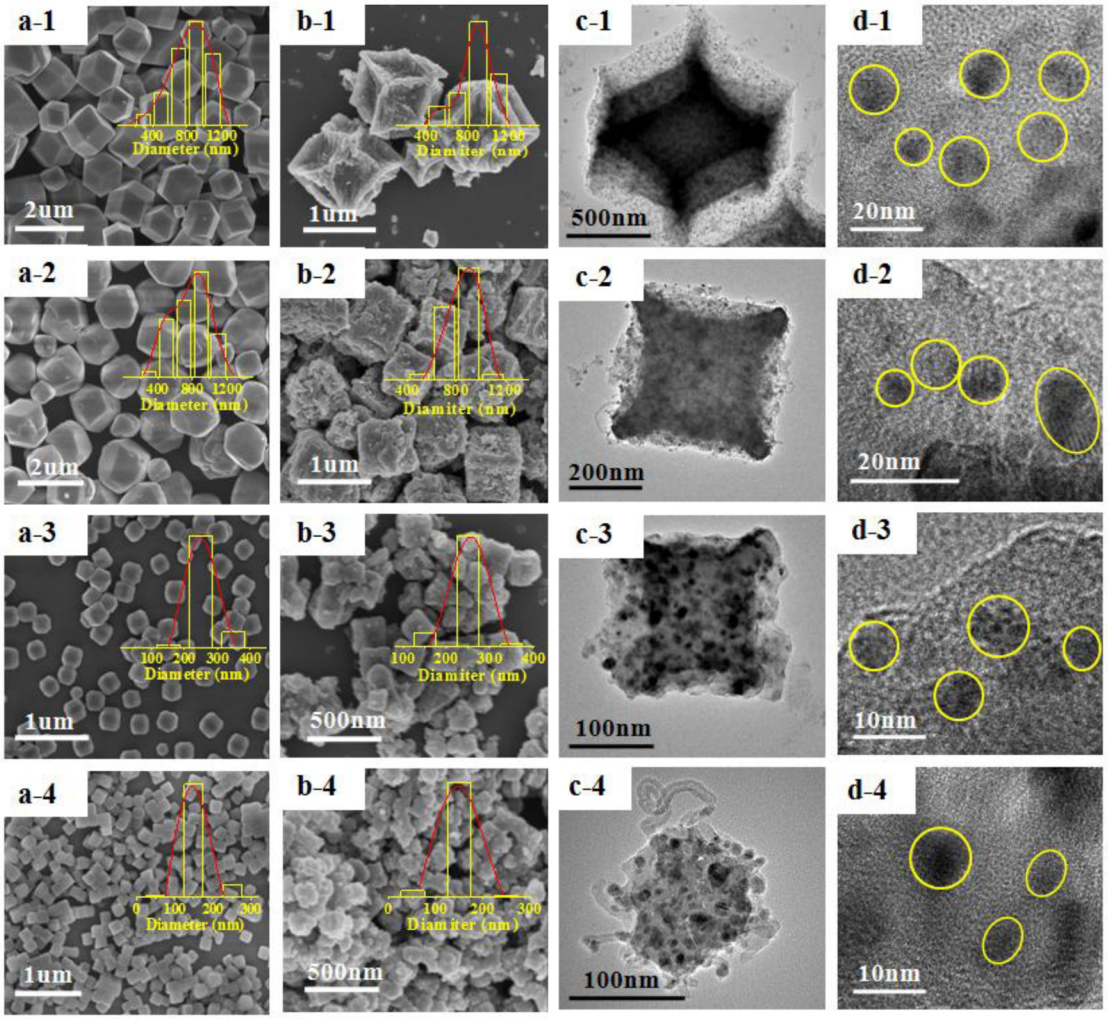


**Figure 2.** SEM and TEM images of ZIF-67 with (a-1) 0 wt %, (a-2) 0.0025 wt %, (a-3) 0.01 wt %, and (a-4) 0.025 wt % CTAB concentrations and their carbonization samples (b, c, d).

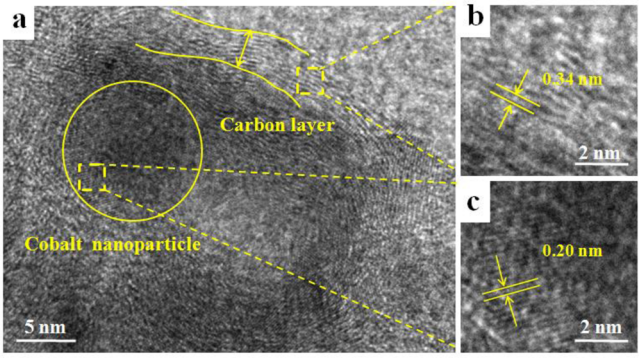


**Figure 3.** TEM images of Co/(0.01)PC-600.

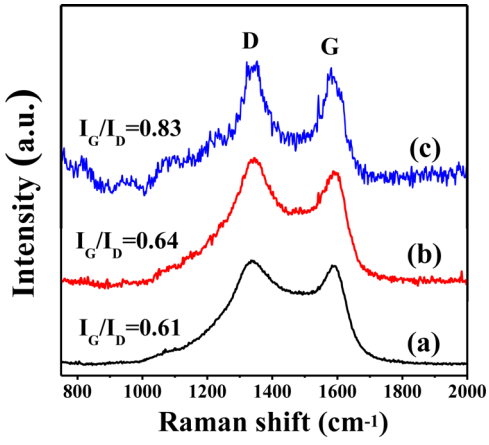


**Figure 4.** Raman spectra of (a) Co/(0.01)PC-600, (b) Co/(0.01)PC-700, and (c) Co/(0.01)PC-800.

in Figure 6. Interestingly, all Co/PCs show higher $CO_2$ uptakes when the precursors contain CTAB; the Co/(0.01)PC-600 exhibits the best $CO_2$ adsorption capacity. The micropore with pore size smaller than a critical value plays an important role in $CO_2$ adsorption.[44] Moreover, Nilantha et al.[45] have found that the small micropore (e.g., <0.8 nm) largely contributes to the $CO_2$ adsorption. Thus, we assume that the small micropore on the Co/(0.01)PC-600 is responsible for the $CO_2$ adsorption capacity and beneficial for the $CO_2$ methanation reaction, which will be discussed in a later section.

**The Catalysis Activity of Co/PC for $CO_2$ Methanation.** The catalytic activity of Co/PC with different morphologies and particle sizes was tested for $CO_2$ methanation at different reaction temperatures (Figures 7 and 8). As seen in Figure 7, as



DOI: 10.1021/acssuschemeng.7b01306
ACS Sustainable Chem. Eng. 2017, 5, 7824−7831

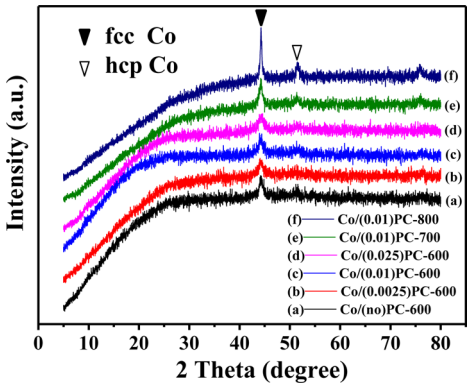


**Figure 5.** XRD patterns of (a) Co/(no)PC-600, (b) Co/(0.0025)PC-600, (c) Co/(0.01)PC-600, (d) Co/(0.025)PC-600, (e) Co/(0.01)PC-700, and (f) Co/(0.01)PC-800.

**Table 2. Physicochemical Properties of Carbonized Co/PC Particles**

| catalyst | $S_{BET}$ [$m^2$ $g^{-1}$] | $V_{pore}$ [$cm^3$ $g^{-1}$] | $V_{micro}$ [$cm^3$ $g^{-1}$] |
|---|---|---|---|
| Co/(no)PC-600 | 243 | 0.12 | 0.090 |
| Co/(0.0025)PC-600 | 295 | 0.16 | 0.107 |
| Co/(0.01)PC-600 | 346 | 0.28 | 0.125 |
| Co/(0.025)PC-600 | 336 | 0.33 | 0.115 |
| Co/(0.01)PC-700 | 343 | 0.27 | 0.082 |
| Co/(0.01)PC-800 | 311 | 0.25 | 0.083 |

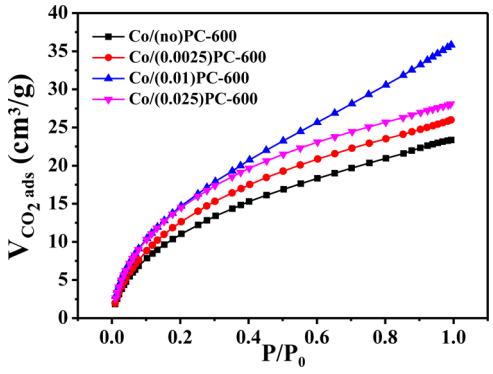


**Figure 6.** $CO_2$ adsorption capacity of Co/PC.

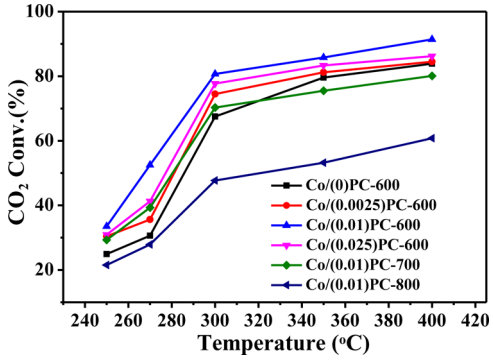


**Figure 7.** $CO_2$ conversion of Co/PC at different reaction temperatures. Reaction conditions: molar ratio of $H_2/CO_2$ = 4/1, GHSV = 72000 mL/($g_{cat}$·h), $P$ = 3 MPa.

the reaction temperatures vary from 250 to 400 °C, the $CO_2$ conversion increases correspondingly with the temperature increasing and closely approaches the equilibrium conversion

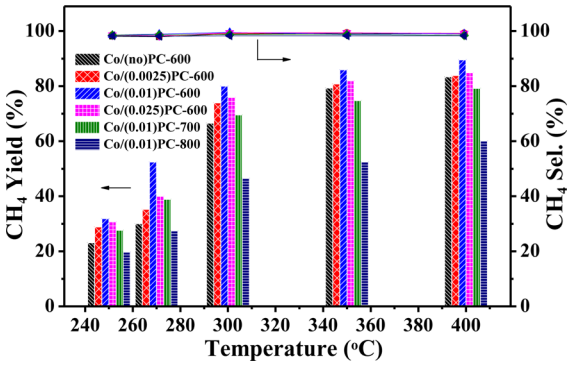


**Figure 8.** $CH_4$ yield and selectivity of Co/PC at different reaction temperatures. Reaction conditions: molar ratio of $H_2/CO_2$ = 4/1, GHSV = 72000 mL/($g_{cat}$·h), $P$ = 3 MPa.

(e.g., 92.8%) at 400 °C. More importantly, the Co/PC catalysts show a promising selectivity to $CH_4$ even as high as 99% at a range of 250 to 400 °C (Figure 8). As the morphologies of Co-based porous carbon change from rhombic dodecahedron to cubic, the $CO_2$ conversion increases remarkably. Above all, when the amount of CTAB is 0.01 wt %, maximum $CO_2$ conversion is observed. Hence, the outstanding performance relates to the CTAB addition. However, the morphology of Co/PC catalysts maintains the cubic, while the microporous volume and $CO_2$ conversion decrease with the CTAB addition up to 0.025 wt %. As mentioned in the section entitled Synthesis and Carbonization of ZIF-67 with Different Crystal Morphologies and Sizes, the maximum microporous volume results in the biggest $CO_2$ adsorption (Figure 6) and undoubtedly promotes $CO_2$ conversion; therefore, the cubic Co/(0.01)PC-600 exhibits the highest $CO_2$ conversion and $CH_4$ yield (Figure 8) at a range of reaction temperature 250 to 400 °C. Particularly, the Co/(0.01)PC-600 shows significant advantage and excellent activity at 270 °C, where the $CO_2$ conversion and $CH_4$ selectivity are 52.5% and 99.2%, respectively. In comparison to prior works, the Co/(0.01)PC-600 exhibits a competitive activity during the Co-based catalysts in the low-temperature (<300 °C) $CO_2$ methanation (see Table 3) even under the 72000 mL $g^{-1}$ $h^{-1}$ GHSV which is much larger than it is in the literature.

**Table 3. Summary of Various Co Catalysts for $CO_2$ Methanation at Low Temperature**

| catalyst | $T$ [°C] | GHSV [mL/($g_{cat}$·h)] | $X_{CO_2}$ [%] | ref |
|---|---|---|---|---|
| Co/KIT-6 | 260 | 22000 | 46 | 21 |
| Co/SSP | 220 | 13200 | 27 | 46 |
| Co/MCM | 220 | 13200 | 28 | 46 |
| Co/TiSSP | 220 | 13200 | 16 | 46 |
| Co/TiMCM | 220 | 13200 | 34 | 46 |
| Co/(0.01)PC-600 | 270 | 72000 | 53 | this work |

To investigate the impact of carbonization temperature on the activity performance of Co/PC catalysts, the most active precursor (0.01CTAB)ZIF-67 was carbonized at 700 and 800 °C, and the tested results for $CO_2$ methanation are depicted in Figures 7 and 8. As the carbonization temperature increases, the $CO_2$ conversion and the $CH_4$ yield decrease, which can be attributed to the sintering of the Co nanoparticles and the decrease of active sites caused by the increasing temperature (Figure 5). Meanwhile, the high carbonization temperature


DOI: 10.1021/acssuschemeng.7b01306
ACS Sustainable Chem. Eng. 2017, 5, 7824−7831

aggravates the graphitization (Figure 4) and sharply decreases the microporous volume (Table 2). One can also see that 600 °C is the optimal carbonization temperature as well as the minimum temperature enabling the decomposition of the zeolitic imidazolate framework.

During the carbonization, some carbon nanotubes were formed where parts of Co nanoparticles were limited in the carbon nanotubes (see Figure S6). To investigate the effect of the confined Co particles on the activity performance, 12 mol/L HCl was used to dissolve the Co nanoparticles inside the carbon matrix of Co/(0.01)PC-600 for 24 h. After an etching treatment with the 12 mol/L HCl, 13.3 wt % of Co remained in comparison to the original level of 32.5 wt % (Table 1). In the meantime, $CO_2$ conversion decreased dramatically from 89% to 2% at 400 °C, which is evidently due to the removal of Co nanoparticles as active sites for $CO_2$ conversion. This result elucidates that the active Co nanoparticle is not the confined Co nanoparticles in the carbon nanotubes.

As a benchmark, the commercially available activated carbon (bought from Shenyang Xinxing Reagent Factory, China) 20 wt % Co loaded was also tested at 400 °C (see Figure 9) (The Co

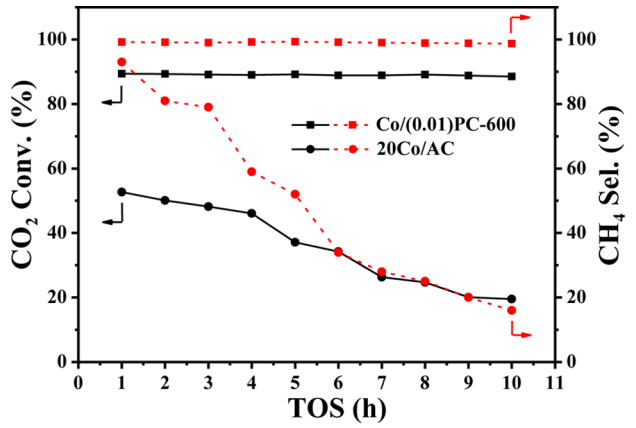


**Figure 9.** $CO_2$ conversion and $CH_4$ selectivity of Co/(0.01)PC-600 and 20Co/AC. Reaction conditions: molar ratio of $H_2/CO_2$ = 4/1, GHSV = 72000 mL/($g_{cat}$·h), $P$ = 3 MPa, $T$ = 400 °C.

content in the Co/(0.01)PC-600 catalyst obtained by TG is 32.5 wt %. However, there was 13.3 wt % Co confined in the carbon nanotubes which was not active for $CO_2$ methanation, so the effective Co content was about 20 and 20 wt % Co loaded on the activated carbon as a benchmark.). At 1 h on stream, the Co/(0.01)PC-600 sample exhibits almost 2 times higher than the 20Co/AC catalyst. Noticeably, the Co/(0.01)PC-600 sample performs a stable $CO_2$ conversion and $CH_4$ selectivity, while the $CO_2$ conversion and $CH_4$ selectivity decrease sharply on the 20Co/AC catalyst. Moreover, the main product of 20Co/AC is CO rather than $CH_4$ at 11 h on stream. Obviously, the Co/PC catalysts performed at a higher activity and stability than the supported catalysts 20Co/AC; during the reaction, the carbon layer in close proximity to the cobalt nanoparticles (Figure 3) resisted the metal sintering effectively.

## CONCLUSION

The ZIF-6-derived Co-based porous carbon catalysts have been synthesized with controlled morphology and size. The crystal morphology of ZIF-67 is regulated from cubic to rhombic dodecahedron, and the particle sizes can be controlled from 150 nm to 1 $\mu$m in an aqueous solution by cetyltrimethylammonium bromide (CTAB) surfactants. After carbonization, the obtained samples inherit the original morphology and size of ZIF-67 crystals with a distorted surface. The Co nanoparticles inside the carbon matrix range from 7 to 20 nm, and they are separated by the graphite-like carbon avoiding the metal sintering effectively. When the amount of CTAB is 0.01 wt %, the carbonized sample possesses the highest BET surface area and micropore volume which also exhibits the highest $CO_2$ adsorption capacity and $CO_2$ methanation activity, especially for the low temperature $CO_2$ methanation at 270 °C. A higher carbonization temperature increases the graphitization degree of the catalysts and decreases the catalytic activity for $CO_2$ methanation. Noticeably, the Co/PC catalysts performed higher activity and stability than the supported catalysts 20Co/AC.

The present work develops a new porous carbon catalyst that comprises highly active Co nanoparticles for $CO_2$ conversion, which shows outstanding methane production activity. The versatile way offers good prospects for low temperature $CO_2$ methanation and prevents metal sintering effectively.

## ASSOCIATED CONTENT

### Supporting Information

The Supporting Information is available free of charge on the ACS Publications website at DOI: 10.1021/acssuschemeng.7b01306.

TG curves of ZIF-67, BET surface area, microporous volume and pore size distribution of ZIF-67 with different amounts of CTAB, SEM-EDS images of Co/(no)PC-600, $H_2$-TPR profiles and pore size distribution of Co/PC samples, enlarged TEM images of Co/(0.0025)PC-600 (PDF)

## AUTHOR INFORMATION

### Corresponding Authors

*Phone: +86-0411-84986133. Fax: 86-0411-84986134. E-mail: guoxw@dlut.edu.cn (X.G.).

*Phone: 814-863-4466. Fax: 814- 865-3573. E-mail: csong@psu.edu (C.S.).

### ORCID

Chunshan Song: 0000-0003-2344-9911

Xinwen Guo: 0000-0002-6597-4979

### Notes

The authors declare no competing financial interest.

## ACKNOWLEDGMENTS

This work was financially supported by the National Key Research and Development Program of China (2016YFB0600902-5).

## REFERENCES

(1) Saeidi, S.; Amin, N. A. S.; Rahimpour, M. R. Hydrogenation of $CO_2$ to Value-Added Products-a Review and Potential Future Developments. *J. $CO_2$ Util.* **2014**, *5*, 66−81.

(2) Rodriguez, J. A.; Liu, P.; Stacchiola, D. J.; Senanayake, S. D.; White, M. G.; Chen, J. G. Hydrogenation of $CO_2$ to Methanol: Importance of Metal-Oxide and Metal-Carbide Interfaces in the Activation of $CO_2$. *ACS Catal.* **2015**, *5*, 6696−6706.

(3) Martin, O.; Martín, A. J.; Mondelli, C.; Mitchell, S.; Segawa, T. F.; Hauert, R.; Drouilly, C.; Curulla-Ferré, D.; Pérez-Ramírez, J. Indium Oxide as a Superior Catalyst for Methanol Synthesis by $CO_2$ hydrogenation. *Angew. Chem., Int. Ed.* **2016**, *55*, 6261−6265.



DOI: 10.1021/acssuschemeng.7b01306
*ACS Sustainable Chem. Eng.* 2017, 5, 7824−7831

(4) Jiang, X.; Koizumi, N.; Guo, X.; Song, C. Bimetallic Pd−Cu Catalysts for Selective $CO_2$ Hydrogenation to Methanol. *Appl. Catal., B* **2015**, *170−171*, 173−185.
(5) Kattel, S.; Yan, B.; Yang, Y.; Chen, J. G.; Liu, P. Optimizing Binding Energies of Key Intermediates for $CO_2$ Hydrogenation to Methanol over Oxide-Supported Copper. *J. Am. Chem. Soc.* **2016**, *138*, 12440−12450.
(6) O'Byrne, J. P.; Owen, R. E.; Minett, D. R.; Pascu, S. I.; Plucinski, P. K.; Jones, M. D.; Mattia, D. High $CO_2$ and Co Conversion to Hydrocarbons Using Bridged Fe Nanoparticles on Carbon Nanotubes. *Catal. Sci. Technol.* **2013**, *3*, 1202−1207.
(7) Lin, Q.; Liu, X.; Jiang, Y.; Wang, Y.; Huang, Y.; Zhang, T. Crystal Phase Effects on the Structure and Performance of Ruthenium Nanoparticles for $CO_2$ Hydrogenation. *Catal. Sci. Technol.* **2014**, *4*, 2058−2063.
(8) Kim, A.; Sanchez, C.; Patriarche, G.; Ersen, O.; Moldovan, S.; Wisnet, A.; Sassoye, C.; Debecker, D. P. Selective $CO_2$ methanation on Ru/$TiO_2$ catalysts: Unravelling the Decisive Role of the $TiO_2$ support Crystal Structure. *Catal. Sci. Technol.* **2016**, *6*, 8117−8128.
(9) Schubert, M.; Pokhrel, S.; Thomé, A.; Zielasek, V.; Gesing, T. M.; Roessner, F.; Mädler, L.; Bäumer, M. Highly Active Co-$Al_2O_3$-Based Catalysts for $CO_2$ methanation with Very Low Platinum Promotion Prepared by Double Flame Spray Pyrolysis. *Catal. Sci. Technol.* **2016**, *6*, 7449−7460.
(10) Wu, H. C.; Chang, Y. C.; Wu, J. H.; Lin, J. H.; Lin, I. K.; Chen, C. S. Methanation of $CO_2$ and Reverse Water Gas Shift Reactions on Ni/$SiO_2$ catalysts: The Influence of Particle Size on Selectivity and Reaction Pathway. *Catal. Sci. Technol.* **2015**, *5*, 4154−4163.
(11) Galletti, C.; Specchia, S.; Saracco, G.; Specchia, V. Co-Selective Methanation over Ru-$\gamma Al_2O_3$ Catalysts in $H_2$-Rich Gas for PEM FC Applications. *Chem. Eng. Sci.* **2010**, *65*, 590−596.
(12) Lunde, P. J.; Kester, F. L. Carbon Dioxide Methanation on a Ruthenium Catalyst. *Ind. Eng. Chem. Process Des. Dev.* **1974**, *13*, 27−33.
(13) Du, G.; Lim, S.; Yang, Y.; Wang, C.; Pfefferle, L.; Haller, G. Methanation of Carbon Dioxide on Ni-Incorporated MCM-41 Catalysts: The Influence of Catalyst Pretreatment and Study of Steady-State Reaction. *J. Catal.* **2007**, *249*, 370−379.
(14) Shin, H. H.; Lu, L.; Yang, Z.; Kiely, C. J.; McIntosh, S. Cobalt Catalysts Decorated with Platinum Atoms Supported on Barium Zirconate Provide Enhanced Activity and Selectivity for $CO_2$ methanation. *ACS Catal.* **2016**, *6*, 2811−2818.
(15) Aziz, M.; Jalil, A. J.; Triwahyono, S.; Mukti, R.; Taufiq-Yap, Y.; Sazegar, M. Highly Active Ni-Promoted Mesostructured Silica Nanoparticles for $CO_2$ Methanation. *Appl. Catal., B* **2014**, *147*, 359−368.
(16) Abdel-Mageed, A. M.; Widmann, D.; Olesen, S. E.; Chorkendorff, I.; Biskupek, J.; Behm, R. J. Selective Co Methanation on Ru/$TiO_2$catalysts: Role and Influence of Metal−Support Interactions. *ACS Catal.* **2015**, *5*, 6753−6763.
(17) Karelovic, A.; Ruiz, P. $CO_2$ Hydrogenation at Low Temperature over Rh/$\gamma$-$Al_2O_3$ Catalysts: Effect of the Metal Particle Size on Catalytic Performances and Reaction Mechanism. *Appl. Catal., B* **2012**, *113−114*, 237−249.
(18) Park, J.; McFarland, E. A Highly Dispersed Pd−Mg/$SiO_2$ Catalyst Active for Methanation of $CO_2$. *J. Catal.* **2009**, *266*, 92−97.
(19) Gao, X.; Liu, H.; Hidajat, K.; Kawi, S. Anti-Coking Ni/$SiO_2$ catalyst for Dry Reforming of Methane: Role of Oleylamine/Oleic Acid Organic Pair. *ChemCatChem* **2015**, *7*, 4188−4196.
(20) Aziz, M.; Jalil, A.; Triwahyono, S.; Ahmad, A. $CO_2$ Methanation over Heterogeneous Catalysts: Recent Progress and Future Prospects. *Green Chem.* **2015**, *17*, 2647−2663.
(21) Zhou, G.; Wu, T.; Xie, H.; Zheng, X. Effects of Structure on the Carbon Dioxide Methanation Performance of Co-Based Catalysts. *Int. J. Hydrogen Energy* **2013**, *38*, 10012−10018.
(22) Zhou, G.; Liu, H.; Cui, K.; Jia, A.; Hu, G.; Jiao, Z.; Liu, Y.; Zhang, X. Role of Surface Ni and Ce Species of Ni/$CeO_2$ Catalyst in $CO_2$ Methanation. *Appl. Surf. Sci.* **2016**, *383*, 248−252.
(23) Wierzbicki, D.; Debek, R.; Motak, M.; Grzybek, T.; Gálvez, M. E.; Da Costa, P. Novel Ni-La-Hydrotalcite Derived Catalysts for $CO_2$ Methanation. *Catal. Commun.* **2016**, *83*, 5−8.
(24) Banerjee, R.; Furukawa, H.; Britt, D.; Knobler, C.; O'Keeffe, M.; Yaghi, O. M. Control of Pore Size and Functionality in Isoreticular Zeolitic Imidazolate Frameworks and Their Carbon Dioxide Selective Capture Properties. *J. Am. Chem. Soc.* **2009**, *131*, 3875−3877.
(25) Rieter, W. J.; Pott, K. M.; Taylor, K. M. L.; Lin, W. Nanoscale Coordination Polymers for Platinum-Based Anticancer Drug Delivery. *J. Am. Chem. Soc.* **2008**, *130*, 11584−11585.
(26) Yaghi, O. M.; O'Keeffe, M.; Ockwig, N. W.; Chae, H. K.; Eddaoudi, M.; Kim, J. Reticular Synthesis and the Design of New Materials. *Nature* **2003**, *423*, 705−714.
(27) Esken, D.; Turner, S.; Lebedev, O. I.; Van Tendeloo, G.; Fischer, R. A. Au@ZIFs: Stabilization and Encapsulation of Cavity-Size Matching Gold Clusters inside Functionalized Zeolite Imidazolate Frameworks, Zifs. *Chem. Mater.* **2010**, *22*, 6393−6401.
(28) Jiang, H.; Liu, B.; Akita, T.; Haruta, M.; Sakurai, H.; Xu, Q. Au@ZIF-8: Co Oxidation over Gold Nanoparticles Deposited to Metal-Organic Framework. *J. Am. Chem. Soc.* **2009**, *131*, 11302−11303.
(29) Zhen, W.; Li, B.; Lu, G.; Ma, J. Enhancing Catalytic Activity and Stability for $CO_2$ Methanation on Ni@MOF-5 Via Control of Active Species Dispersion. *Chem. Commun.* **2015**, *51*, 1728−1731.
(30) Hu, S.; Liu, M.; Ding, F.; Song, C.; Zhang, G.; Guo, X. Hydrothermally Stable MOFs for $CO_2$ Hydrogenation over Iron-Based Catalyst to Light Olefins. *J. $CO_2$ Util.* **2016**, *15*, 89−95.
(31) Shen, K.; Chen, L.; Long, J.; Zhong, W.; Li, Y. MOFs-Templated Co@Pd Core−Shell Nps Embedded in N-Doped Carbon Matrix with Superior Hydrogenation Activities. *ACS Catal.* **2015**, *5*, 5264−5271.
(32) Hong, S.; Yoo, J.; Park, N.; Lee, S. M.; Park, J. G.; Park, J. H.; Son, S. U. Hollow Co@C Prepared from a Co-ZIF@Microporous Organic Network: Magnetic Adsorbents for Aromatic Pollutants in Water. *Chem. Commun.* **2015**, *51*, 17724−17727.
(33) Zhou, Y. X.; Chen, Y. Z.; Cao, L.; Lu, J.; Jiang, H. L. Conversion of a Metal-Organic Framework to N-Doped Porous Carbon Incorporating Co and CoO Nanoparticles: Direct Oxidation of Alcohols to Esters. *Chem. Commun.* **2015**, *51*, 8292−8295.
(34) Torad, N. L.; Hu, M.; Ishihara, S.; Sukegawa, H.; Belik, A. A.; Imura, M.; Ariga, K.; Sakka, Y.; Yamauchi, Y. Direct Synthesis of MOF-Derived Nanoporous Carbon with Magnetic Co Nanoparticles toward Efficient Water Treatment. *Small* **2014**, *10*, 2096−2107.
(35) Xu, D.; Zhang, D.; Zou, H.; Zhu, L.; Xue, M.; Fang, Q.; Qiu, S. Guidance from an in Situ Hot Stage in Tem to Synthesize Magnetic Metal Nanoparticles from a MOF. *Chem. Commun.* **2016**, *52*, 10513−10516.
(36) Pan, Y.; Heryadi, D.; Zhou, F.; Zhao, L.; Lestari, G.; Su, H.; Lai, Z. Tuning the Crystal Morphology and Size of Zeolitic Imidazolate Framework-8 in Aqueous Solution by Surfactants. *CrystEngComm* **2011**, *13*, 6937−6940.
(37) Guo, X.; Xing, T.; Lou, Y.; Chen, J. Controlling ZIF-67 Crystals Formation through Various Cobalt Sources in Aqueous Solution. *J. Solid State Chem.* **2016**, *235*, 107−112.
(38) Li, K.; Olson, D. H.; Seidel, J.; Emge, T. J.; Gong, H.; Zeng, H.; Li, J. Zeolitic Imidazolate Frameworks for Kinetic Separation of Propane and Propene. *J. Am. Chem. Soc.* **2009**, *131*, 10368−10369.
(39) Pham, M.; Vuong, G.; Vu, A.; Do, T. Novel Route to Size-Controlled Fe-MIL-88B-$NH_2$ Metal-Organic Framework Nanocrystals. *Langmuir* **2011**, *27*, 15261−15267.
(40) Cai, X.; Lin, J.; Pang, M. Facile Synthesis of Highly Uniform Fe-MIL-88B Particles. *Cryst. Growth Des.* **2016**, *16*, 3565−3568.
(41) Shi, Q.; Chen, Z.; Song, Z.; Li, J.; Dong, J. Synthesis of ZIF-8 and ZIF-67 by Steam-Assisted Conversion and an Investigation of Their Tribological Behaviors. *Angew. Chem., Int. Ed.* **2011**, *50*, 672−675.
(42) Park, K.; Ni, Z.; Cote, A.; Choi, J.; Huang, R.; Uribe-Romo, F.; Chae, H.; O'Keeffe, M.; Yaghi, O. M. Exceptional Chemical and Thermal Stability of Zeolitic Imidazolate Frameworks. *Proc. Natl. Acad. Sci. U. S. A.* **2006**, *103*, 10186−10191.


DOI: 10.1021/acssuschemeng.7b01306
*ACS Sustainable Chem. Eng.* 2017, 5, 7824−7831

(43) Pei, Y.; Li, Z.; Li, Y. Highly Active and Selective Co-Based Fischer−Tropsch Catalysts Derived from Metal-Organic Frameworks. *AIChE J.* **2017**, *63*, 2935−2944.
(44) Zhang, Z.; Zhou, J.; Xing, W.; Xue, Q.; Yan, Z.; Zhuo, S.; Qiao, S. Z. Critical Role of Small Micropores in High $CO_2$ Uptake. *Phys. Chem. Chem. Phys.* **2013**, *15*, 2523−2529.
(45) Wickramaratne, N.; Jaroniec, M. Importance of Small Micropores in $CO_2$ capture by Phenolic Resin-Based Activated Carbon Spheres. *J. Mater. Chem. A* **2013**, *1*, 112−116.
(46) Janlamool, J.; Praserthdam, P.; Jongsomjit, B. Ti-Si Composite Oxide-Supported Cobalt Catalysts for $CO_2$ Hydrogenation. *J. Nat. Gas Chem.* **2011**, *20*, 558−564.



DOI: 10.1021/acssuschemeng.7b01306
*ACS Sustainable Chem. Eng.* 2017, 5, 7824−7831